Research Article
Experimental and Translational Hepatology

JOURNAL
OF HEPATOLOGY

Spatiotemporal liver dynamics shape hepatocellular heterogeneity and impact *in vivo* gene engineering

Authors

Michela Milani, Francesco Starinieri, Stefano Beretta, …, Matteo Iannacone, Ivan Merelli, Alessio Cantore

Correspondence

cantore.alessio@hsr.it (A. Cantore).

Graphical abstract

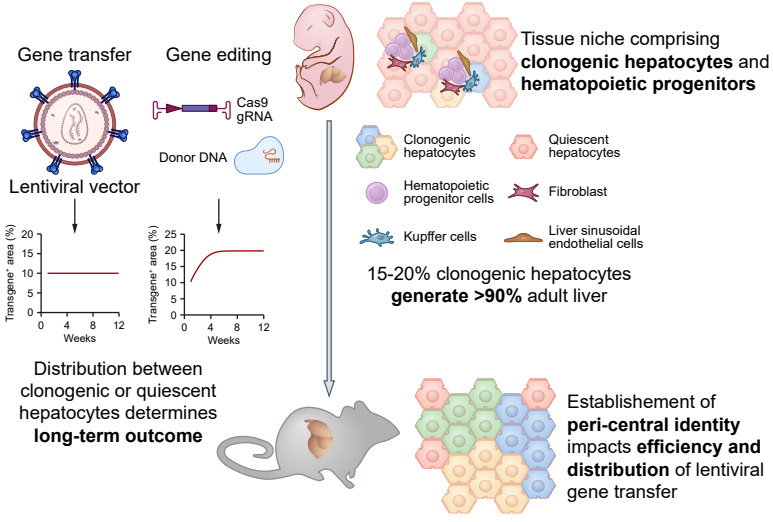

Highlights

- Most adult liver arises from a small fraction of clonogenic newborn hepatocytes.
- Preferential editing of clonogenic hepatocytes expands the edited liver area.
- The peri-central hepatocyte identity is established after weaning.
- The efficiency and localization of lentiviral gene transfer depend on age at treatment.
- Clonogenic hepatocytes co-localize with hematopoietic islands in the neonatal liver.

Impact and implications

We provide new insights into the spatiotemporal dynamics of the mouse liver during postnatal growth, highlighting both proliferative and transcriptomic heterogeneity among hepatocytes and their impact on the efficiency and distribution of *in vivo* lentiviral gene delivery and targeted gene editing. Understanding and manipulating the biological processes behind this heterogeneity can enhance gene transfer outcomes. We report that not all hepatocytes contribute equally to liver growth, indicating that effectively targeting clonogenic hepatocytes in the newborn liver is crucial for the long-term maintenance of therapeutic genetic modifications. Furthermore, this phenomenon can be leveraged to expand the pool of genetically corrected cells, as illustrated here by a targeted gene editing strategy. Finally, we reveal the existence of a tissue niche that supports the proliferation of both clonogenic hepatocytes and hematopoietic progenitors in neonatal livers. Gaining a deeper understanding of this niche and its signals may be beneficial for regenerative purposes.

https://doi.org/10.1016/j.jhep.2025.06.018
 J. Hepatol. 2025, 83, 1392–1409

Research Article
Experimental and Translational Hepatology

JOURNAL
OF HEPATOLOGY

Spatiotemporal liver dynamics shape hepatocellular heterogeneity and impact *in vivo* gene engineering

Michela Milani[1,†], **Francesco Starinieri**[1,2,†], Stefano Beretta[1], Marco Monti[1], Cesare Canepari[1], Francesca Marabotti[1,2], Samuel Zambrano[2,3], Davide Mazza[2,3], Anna Fabiano[1], Chiara Simoni[1,2], Eugenia Cammarota[3], Monica Volpin[1], Giulia Bortolussi[4], Fabio Russo[1], Mauro Biffi[1], Marco Genua[1], Sara Degl'Innocenti[1], Francesca Sanvito[1], Renato Ostuni[1], Andrés F. Muro[4], Eugenio Montini[1], Federica Moalli[3], Matteo Iannacone[2,3], Ivan Merelli[5], Alessio Cantore[1,2,*]

Journal of Hepatology **2025**. vol. 83 | 1392–1409

Check for updates

See Editorial, pages 1253–1255

Background & Aims: Hepatocytes are the liver's main functional cells and are key targets for *in vivo* gene therapy to treat monogenic diseases. Integrating the transgene into the genome is critical for long-term expression from a single early-life dose, which is achievable via integrating vectors or genome editing. To ensure persistence through liver growth and cell turnover, it is also necessary to target the hepatocytes driving these processes. While liver regeneration and homeostasis have been studied extensively, hepatocyte growth and maturation remain less well understood. Here, we investigate how hepatocyte heterogeneity evolves during liver growth and its implications for *in vivo* gene engineering.

Methods: We performed clonal tracing, as well as single-cell and spatial transcriptomics, on mouse livers of various ages. We evaluated the efficiency, stability, and lobule distribution of lentiviral gene transfer and targeted transgene integration.

Results: We found that a subset of clonogenic hepatocytes (15-20%) in the newborn liver generates >90% of the adult tissue and co-localizes with hematopoietic islands within a spatial niche. Preferential gene editing of these clonogenic hepatocytes resulted in an increased proportion of the gene-engineered liver area, supporting their role in liver growth. Age-dependent hepatocellular heterogeneity affected the efficiency of lentiviral gene delivery *in vivo* and its distribution throughout the hepatic lobule. The gradual establishment of metabolic zonation after weaning and elevated proteasome activity in the peri-central area in adults influenced the observed age-related outcomes.

Conclusion: These insights into spatiotemporal hepatocyte dynamics enhance our understanding of liver biology and have important implications for therapeutic strategies.

Introduction

The liver plays a central role in several physiological processes, including the metabolism of biological molecules and xenobiotics, as well as the biosynthesis and secretion of plasma proteins. Hepatocytes, the most abundant cells in the liver, are responsible for most of these functions. Although they are morphologically similar, adult hepatocytes are functionally heterogeneous, based on their position in the liver lobule, a concept known as zonation.[1,2] Various metabolic processes are primarily described as occurring in hepatocytes situated near the portal areas (peri-portal [PP]), or near the central vein (peri-central [PC]). Hepatocytes significantly proliferate during postnatal liver growth, acquiring a mature phenotype,[3] and then maintain tissue homeostasis in adulthood while exhibiting considerable regenerative capacity following damage.[4] Although liver homeostasis and regeneration have been extensively studied, the processes of liver growth and maturation are not as well understood. Studies based on retrospective radiocarbon dating estimate that hepatocytes in the human liver divide at a rate of 17-19% per year in adults.[5] Recent research has shown that hepatocytes involved in liver turnover are distributed throughout the lobule, and that midlobular hepatocytes may primarily contribute to homeostatic proliferation.[6–9] Additionally, studies on liver regeneration have identified several contributing cell types, including hepatocytes and biliary epithelial cells.[10–14] However, there is limited

* Corresponding author. Address: San Raffaele Telethon Institute for Gene Therapy, IRCCS San Raffaele Scientific Institute, Via Olgettina 58, Milan, Italy.
E-mail address: cantore.alessio@hsr.it (A. Cantore).
† Equal contribution
https://doi.org/10.1016/j.jhep.2025.06.018

knowledge regarding postnatal liver growth, particularly concerning whether and how distinct hepatocyte subpopulations contribute to this process. Furthermore, the dynamics of acquiring mature phenotypes remain to be fully elucidated.

Understanding liver tissue dynamics is also relevant for the safety, efficiency, and durability of genetic engineering strategies targeting the liver for therapeutic purposes. Mutations in genes expressed by hepatocytes can lead to various monogenic diseases, such as plasma protein deficiencies (*e.g.* hemophilia) and metabolic disorders that may potentially be treated through *in vivo* liver-directed gene therapy.[15] Recombinant adeno-associated virus (AAV)-derived vectors have emerged as the most advanced platform for this purpose, as testified by multi-year therapeutic benefits in adults, achieved after a single i.v. administration, leading to the availability of commercial gene therapies for adult patients with hemophilia.[16,17] The success of AAV-vector-based liver gene therapy in adults has prompted exploration into extending its application to pediatric patients. However, AAV vectors do not actively integrate into the host cell genome, which leads to decreased therapeutic efficacy following cell proliferation, such as during liver growth and homeostatic renewal. To overcome this limitation, methods for stable modification of the genome, such as integrating viral vectors or gene editing, are preferred to achieve a once-in-a-lifetime treatment for monogenic diseases affecting young patients. Lentiviral vectors (LV), which integrate into the target cell chromatin and are maintained through cell division, have shown potential for achieving stable and possibly lifelong transgene expression. In both small and large animal models, i.v. administration of LV resulted in stable liver gene transfer, allowing long-term correction of hemophilia and metabolic diseases in both adult and newborn individuals.[18–22] Gene editing, particularly with CRISPR/Cas9 technology, offers the prospect of site-specific modification of the genome.[23] This process involves providing target cells with programmable nucleases like CRISPR/Cas9, along with a template DNA containing homology for the nuclease's genomic target site, thereby promoting targeted integration through homology-directed repair (HDR). *In vivo* gene editing has been successfully performed in hepatocytes to treat inherited metabolic diseases and hemophilia.[24–28] Regardless of the genetic engineering tool used, the ultimate goal of liver gene therapy for monogenic diseases is to provide safe, therapeutic, lifelong replacement of the missing function to pediatric patients through a single administration. Therefore, it is essential to ensure that the genetic modification is efficiently delivered and sustained in the hepatocytes that contribute to liver growth and homeostatic renewal.

Herein, we investigate the dynamics of postnatal liver tissue through clonal analysis and spatial transcriptomics. We report that a relatively small fraction of newborn hepatocytes is responsible for generating the majority of adult liver mass. These cells initially share an instructive tissue niche with hematopoietic progenitors in neonatal mouse livers and progressively acquire a PC identity, significantly affecting the efficiency and stability of *in vivo* hepatocyte genetic engineering.

Materials and methods

The materials and methods are provided in the supplementary information.

Results

Most adult liver tissue originates from a subset of clonogenic hepatocytes in newborns

We initially aimed to assess the proliferation of hepatocytes in mice during postnatal liver growth. We evaluated the clonal proliferation of hepatocytes in mice expressing a tamoxifen-inducible Cre recombinase controlled by the hepatocyte-specific albumin promoter (*Alb.CreERT2*) and carrying the Confetti reporter (*R26-Confetti)*,[29] in which one out of four different fluorescent markers is activated following Cre-mediated recombination. We activated Cre by administering tamoxifen to these newborn mice (postnatal day 1, D1) and analyzed their livers by immunofluorescence at various times post-activation (Figs. 1A and S1A). We did not detect Confetti-positive hepatocytes in mice that did not receive tamoxifen (Fig. S1B) and observed approximately 20% recombination efficiency, maintained stably throughout liver growth (Fig. S1C). We noted a gradual increase in the average size of hepatocyte groups (referred to as clusters), identified by a single color (Fig. 1B). In the first 6 weeks of life, there was an 8-fold increase in the average cluster size, but between week 6 and 1 year, the increase was less than 2-fold, indicating a reduced proliferation rate during adulthood. We estimated the number of hepatocytes per cluster based on the average cell size at each age of analysis. Notably, we found that about 75% of clusters consisted of 1-2 cells throughout liver growth and homeostasis, while the remaining 25% seemed to proliferate and generate progressively larger clusters (Fig. 1C). The marked tissue area occupied by clusters of >2 cells progressively increased, reaching >90% of the adult liver (Fig. 1D). These data suggest that most hepatocytes in the newborn liver remain quiescent or slowly replicating, while around 25% of them form continuously growing clusters, covering 90% of the adult liver area. A few very large clusters (>50 cells) emerged in mice at 6 weeks or 1 year (Fig. 1E). To complement this analysis, we administered Cre recombinase to newborn Confetti mice through mRNA delivery mediated by lipid nanoparticles. This approach allowed for a shorter duration of Cre expression compared to tamoxifen-mediated induction of CreERT2 activity. In fact, the initial recombination efficiency was lower than that observed in the previous set of experiments (4%). We monitored the size and growth of the hepatocyte clusters until 6 weeks of age and confirmed that approximately 80% of the clusters remained the smallest size (1-2 cells), consistent with the previous analysis (Fig. S1D-F). Interestingly, at 6 weeks of age, the clusters were, on average, smaller than those in *Alb.CreERT2/R26-Confetti* mice, suggesting that some fusions of nearby clusters occurred in the latter experimental setting due to the higher initial marking efficiency.

We then activated Cre recombination by administering tamoxifen to juvenile (2-week-old, W2) *Alb.CreERT2/R26-Confetti* mice. Unlike our observations in newborn mice, marking hepatocytes in 2-week-old mice showed a mild 2-fold increase in cluster average size over time, with the percentage of marked area made up of expanding clusters (>2 cells) at 60% instead of 90% at 1 year (Fig. S1G–I). These data suggest that the proliferation rate of hepatocytes is already reduced by the second week of age. We also marked hepatocytes in adult

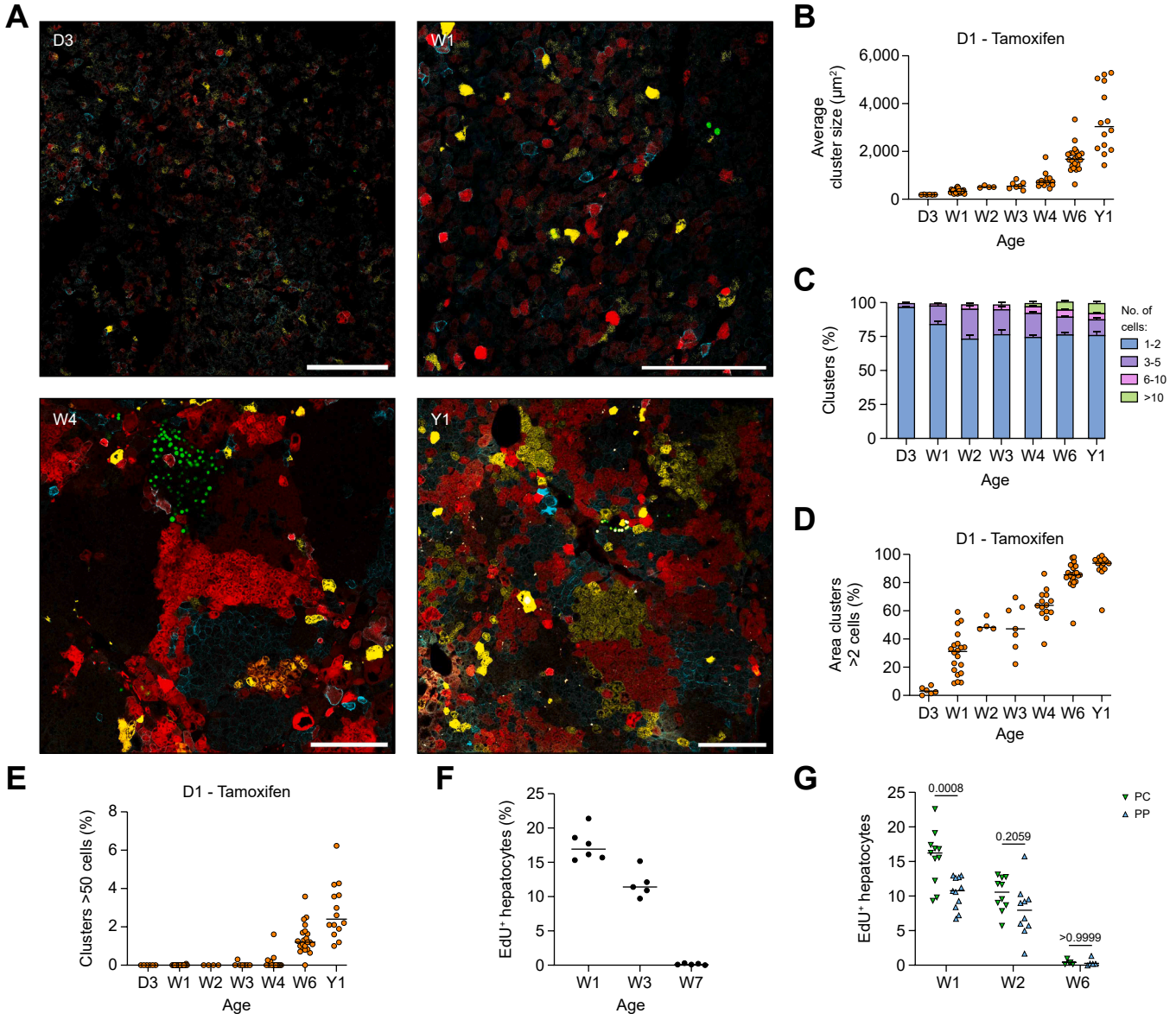

Fig. 1. Only a fraction of hepatocytes proliferate in the newborn liver. (A) Representative images of *Alb.CreERT2/R26-Confetti* mice treated with a single dose of tamoxifen (0.1 mg/g), administered subcutaneously when newborns (D1), and analyzed on postnatal day 3 (D3), week 1 (W1), week 4 (W4), or 1 year of age (Y1). Scale bar: 200 µm. (B) Individual values and median of average cluster sizes marked by one Confetti fluorescent reporter (RFP, YFP, or CFP; GFP is excluded from the analysis due to its nuclear localization). Mice were analyzed at the specified time points. D3 n = 6; W1 n = 20; W2 n = 4; W3 n = 7; W4 n = 14; W6 n = 22; Y1 n = 14. (C) Mean with SEM of the percentage of Confetti-positive clusters consisting of 1-2, 3-5, 6-10, or >10 cells from the mice in (B). (D) Individual values and median of the percentage of Confetti-positive area constituted by clusters with >2 cells from the mice in (B). (E) Individual values and median of the percentage of Confetti-positive clusters composed of >50 cells from the mice in (B). (F, G) Individual values and median of the percentage of hepatocytes (HNF4α-positive) marked by EdU (F) and their PC or PP localization within the liver lobule. Mice received three doses of EdU during the first week (W1, postnatal days 2, 3, and 4, n = 6), the third week (W3, postnatal days 14, 15, and 16, n = 5), or the seventh week (W7, postnatal days 42, 43, and 44, n = 5) of life and were analyzed 1 day after the last dose of EdU. Mann-Whitney test. CFP, cyan fluorescent protein; EdU, 5-ethynyl-2'-deoxyuridine; GFP, green fluorescent protein; PC, pericentral; PP, periportal; RFP, red fluorescent protein; YFP, yellow fluorescent protein.

Alb.CreERT2/R26-Confetti mice (at 8±2 weeks of age). In this case, we observed only a very mild increase in the average size of clusters over time. The percentage of clusters with more than two cells was 10-20% at year 1, while the marked area consisting of expanding clusters was 30% at year 1 (Fig. S1J-L). To further quantify replicating hepatocytes, we administered 5-Ethynyl-2′-deoxyuridine (EdU) to wild-type (WT) mice of various ages. Within the first week of life, 15-20% of hepatocytes were EdU positive, decreasing to 10-15% by week 3 and <1% during week 7 (Fig. 1F). Thus, we confirmed a reduction in hepatocyte proliferation rate over time, already at 2 weeks of age and consistent with the very slow turnover of hepatocytes during homeostasis in the adult mouse liver.[7] Additionally, we observed a slight enrichment of EdU-positive hepatocytes in the PC area (Fig. 1G). Collectively, these data indicate that approximately 15-20% of hepatocytes proliferate in the newborn liver, leading to over 90% of the adult liver, through growing clusters that proliferate at a progressively slower rate.

Based on these data, we set out to mathematically model hepatocyte proliferation throughout liver growth. We assigned three possible states to hepatocytes, meaning the total number N is NP + Q + R, where Q represents quiescent hepatocytes, P denotes hepatocytes with proliferative potential (*i.e.*, clonogenic), and R indicates replicating hepatocytes (*i.e.*, actively cycling P hepatocytes). In this simple model, the proliferative hepatocytes can become replicating (splitting into two proliferative hepatocytes) or irreversibly enter the quiescent state (Fig. S2A). Importantly, we assume that the probability of transitioning from P to R approaches zero as N approaches its maximum (N_{max}), analogous to the well-known logistic model,[30] proposed for scenarios where resources and growth factors are limited.[31] We estimated N based on the average number of hepatocytes per gram of liver ($1.3x10^8$)[32] and by weighing the liver at various ages during liver growth in WT mice (Fig. S2B and C). Remarkably, this relatively simple mathematical model well fitted the experimental data collected in Confetti and WT mice, particularly, the number N of hepatocytes over time, the percentage of replicating hepatocytes, and the area of the liver covered by the initially quiescent hepatocytes (Fig. S2D and E). As proliferating hepatocytes asymptotically tend to 0 over time, we simulated 30% hepatectomy at week 8 and showed that the remaining proliferating hepatocytes re-acquired a replicative state and gradually regenerated liver mass, suggesting that our simple model can also reproduce the adult liver's regenerative ability (Fig. S2F). We then stochastically simulated the growth of 100 hepatocyte clusters, each starting from a single cell, and compared the cluster size distribution predicted by the model (Fig. S2G and H) with that obtained experimentally in Confetti mice (see Fig. 1C). We observed a highly similar pattern, despite variations in the medium-sized clusters. Overall, the good concordance of the mathematical modeling and experimental data supports the proposed mechanism that a fraction of newborn hepatocytes generates most of the adult liver. These data prompted us to characterize the transcriptional profile of hepatocytes in the liver of newborn mice.

Single-nuclei transcriptomic analysis highlights proliferative heterogeneity among newborn hepatocytes

We performed single-nuclei RNA sequencing (snRNA-seq) on three livers from WT newborn mice. Through unsupervised clustering, we identified the major liver cell populations (Fig. 2A). The two most abundant clusters consisted of hepatocytes and hematopoietic stem/progenitor cells (HSPCs), indicating the persistence of residual fetal hematopoiesis in the newborn liver. We concentrated on hepatocytes and identified seven subclusters, characterized by subtle yet significant transcriptome variations (Fig. 2B). We confirmed the stability and reproducibility of the hepatocyte subclusters via a dedicated bioinformatic analysis (Fig. S3A). We found that 23% of hepatocytes were positive for *Mki67*, indicating their cycling state, which is consistent with the results presented above. We stratified the hepatocytes based on *Mki67* expression (Fig. 2C, D) and subsequently conducted gene set-enrichment analysis (GSEA) on the two *Mki67*-high clusters (4 and 5). GSEA revealed an upregulation of cell cycle genes, confirming the proliferative state of the cells, along with a downregulation of pathways characteristic of hepatocyte identity, such as those involved in xenobiotic, cholesterol, and bile acid metabolism, as well as coagulation (Fig. 2E). Consistent with this analysis, the expression of albumin and other hepatocyte-specific genes was highest in the hepatocyte subsets characterized by lower *Mki67* expression (Figs 2F,G and S3B-E), suggesting a less differentiated state for the more proliferating hepatocytes. Interestingly, heme metabolism emerged as an enriched pathway in the most proliferative hepatocytes (see Fig. 2E). To confirm the identity of the identified clusters, we verified the absence of hepatocyte gene expression in HSPCs as a negative control while confirming their expression in proliferating cluster-5 hepatocytes (Fig. S3F). We also validated the differential expression of selected genes between proliferating and quiescent hepatocyte subsets at the protein level using spectral flow cytometry analysis (Fig. S3G). Next, we aimed to evaluate how this differential proliferation state of neonatal hepatocytes affects the maintenance of *in vivo* genetic engineering by employing HDR-based gene editing and semi-randomly integrating LV, taken as representative of integrative gene therapy strategies.

The initial distribution of genetic modification between proliferating and non-proliferating hepatocytes determines the extent of the genetically engineered area at the end of liver growth

We first determined whether gene editing via HDR was enriched in proliferating hepatocytes in newborn mice. We co-administered i.v. two AAV vectors ($2x10^{14}$ vector genomes/kg each), one expressing Cas9 and a guide RNA targeting the 3' untranslated region of the albumin gene, and the other one delivering a donor DNA carrying a mCherry transgene preceded by the self-cleaving 2A peptide and flanked by sequences homologous to the targeted genomic site, to WT mice at D1 of age (Fig. 3A). In this strategy, mCherry is expressed only if it is properly inserted in-frame just upstream of the albumin stop codon, by HDR.[26,33] We observed 10% of mCherry-positive hepatocytes, higher than in control mice, administered without CRISPR/Cas9-expressing AAV (Fig. 3B), in line with a previous report.[26] To monitor the proliferation of hepatocytes, we administered EdU concurrently with the two AAV vectors and over the next 2 days. We observed >4-fold higher percentage of EdU-positive hepatocytes in mCherry-positive compared to total hepatocytes (Fig. 3C), indicating that HDR occurred preferentially, though not exclusively, in proliferating hepatocytes in newborn mice. This resulted in a doubling of the percentage of mCherry-positive tissue area at the end of liver growth (Fig. 3D). These data show that *in vivo* HDR-mediated gene editing is enriched in proliferating hepatocytes of newborn mice, leading to an expansion of the proportion of the gene-edited area. We thus exploited the mathematical model of hepatocyte proliferation described above, to simulate how the genetically modified area would change over time given the observed distribution of proliferating hepatocytes between gene-edited (45%) and non-modified (15%) hepatocytes (see Fig. 3C). Also in this case, the model prediction overlapped the experimental observation (Fig. 3E,F).

In parallel, we used LV to efficiently integrate transgenes, modeling a gene addition strategy. We i.v. administered a VSV. G (vesicular stomatitis virus G protein)-pseudotyped LV

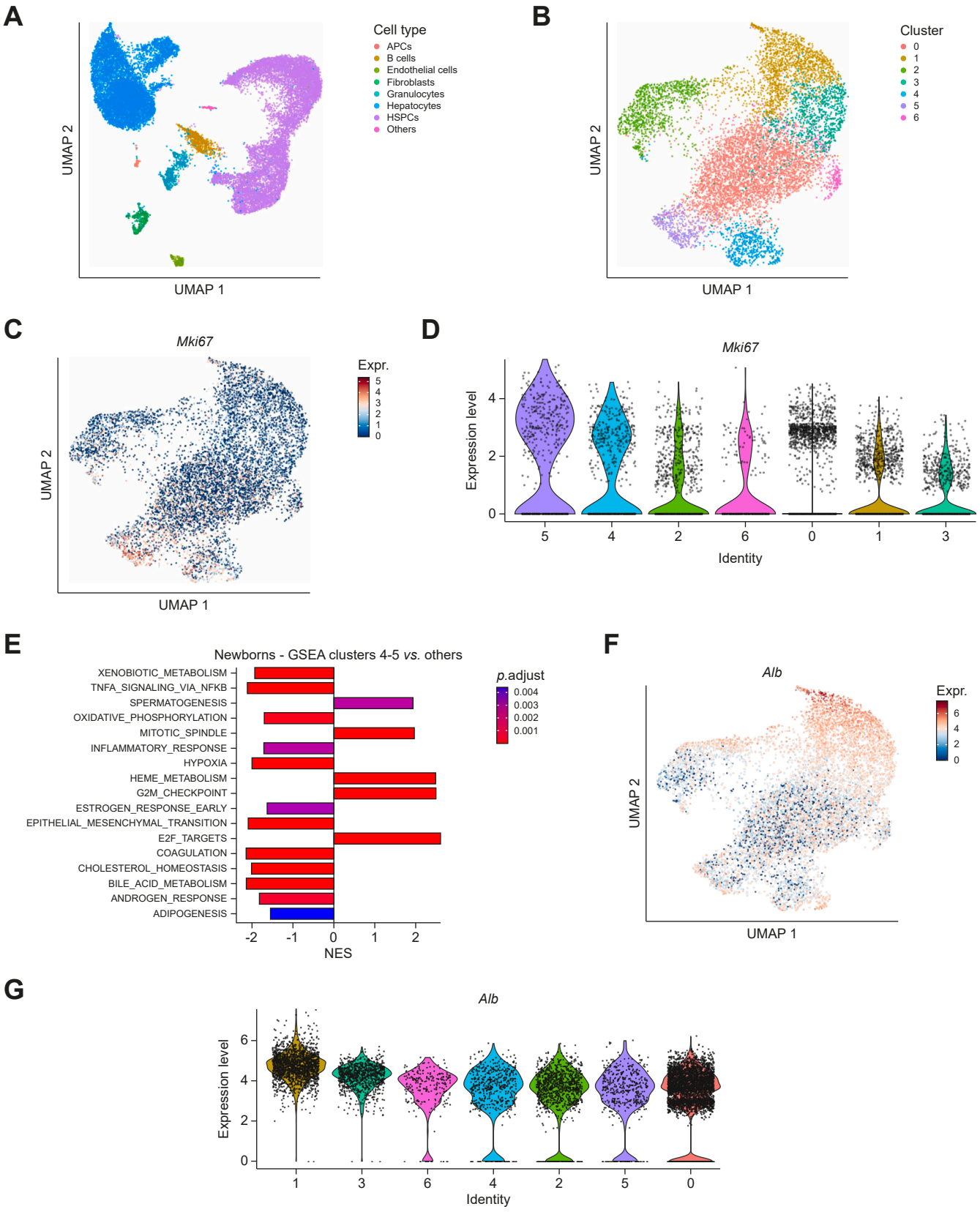

Fig. 2. Transcriptomic analysis of the newborn liver reveals a subset of less differentiated, proliferating hepatocytes. (A) UMAP plot of snRNA-seq from three newborn livers, colored according to unsupervised clustering. (B, C) UMAP of single nuclei identified as hepatocytes in (A), colored based on unsupervised clustering (B), or displaying expression of the *Mki67* gene (C). (D) Violin plot of *Mki67* expression in each cluster shown in (B). (E) GSEA on *Mki67*-high clusters 4-5 compared to all other clusters from the unsupervised clustering (see panel B). The x-axis presents the NES. The bar plot is colored according to the adjusted *p* value (*p*.adjust). (F)

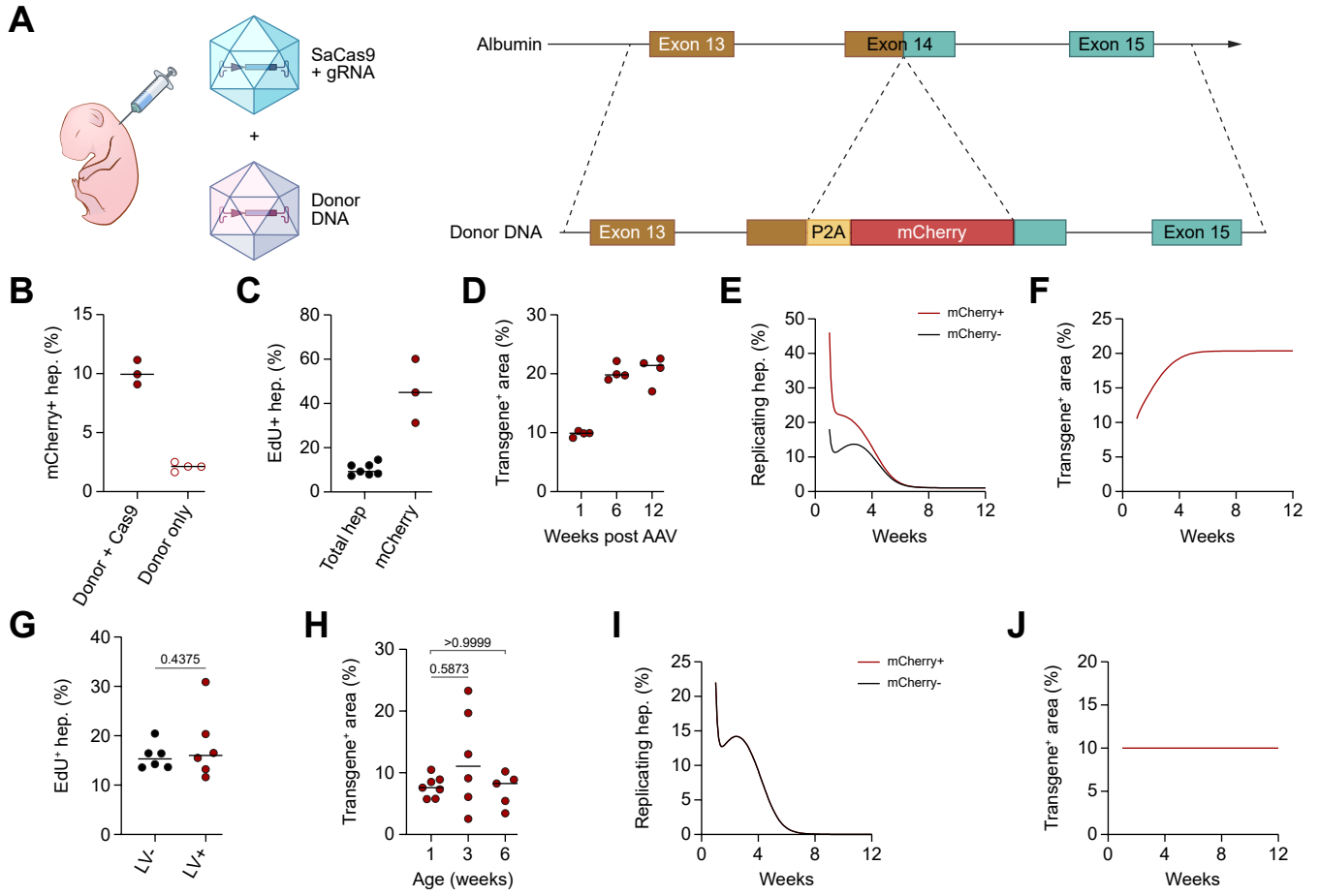

Fig. 3. HDR-based gene editing preferentially occurs in proliferating hepatocytes, leading to the enrichment of the edited area during postnatal growth. (A) Experimental scheme: newborn mice are treated with 2 AAV vectors ($4.5x10^{11}$ vg/mouse each), one of which codes for *Staphylococcus aureus* Cas9 and gRNA targeting the stop codon of the albumin gene, while the other carries donor DNA with homology arms to mediate the integration of the P2A.mCherry transgene in-frame with the last coding exon of the albumin gene. (B) Single values and median of the mCherry-positive area of mice treated at D1 with Cas9-encoding AAV and donor DNA AAV, or donor DNA AAV only, followed by three doses of EdU at D1, D2, and D3, then analyzed at D5. Donor+Cas9 n = 3, Donor only n = 3. (C) Single values and median of the percentage of hepatocytes marked by EdU in mice from (B). (D) Single values and median of the liver transgene-positive area measured 1-, 6- or 12-weeks post i.v. administration of Cas9 AAV and donor DNA AAV to mice at D1. 1 week n = 4, 6 weeks n = 4, 12 weeks n = 4. (E, F) Mathematical modeling (see Fig. S2) of the percentage of replicating mCherry-positive or -negative hepatocytes (E), or of the transgene-positive area (F) over time, starting from 45% of replicating hepatocytes in the mCherry-positive group as shown in (C). (G) Single values and median of the percentage of hepatocytes marked by EdU 1 week after i.v. administration of LV to mice at D1 ($2.5x10^{10}$ transducing units/kg, n = 6). Wilcoxon matched-pairs signed-rank test. (H) Single values and median of the liver transgene-positive area measured 1, 3 or 6 weeks post-LV administration. 1 week n = 7, 3 weeks n = 6, 6 weeks n = 5. Kruskal-Wallis test with Dunn's multiple comparisons test. (I, J) Mathematical modeling (see Fig. S2) of the percentage of replicating mCherry-positive or -negative hepatocytes (I), or of the transgene-positive area (J) over time, starting from the same frequency of replicating hepatocytes in the mCherry-positive or -negative group as in (G). AAV, adeno-associated virus; Alb, albumin; Cas9, CRISPR-associated protein 9; D1, day 1; D2, day 2; D3, day 3; D5, day 5; EdU, 5-ethynyl-2'-deoxyuridine; gRNA, guide RNA; HDR, homology-directed repair; LV, lentiviral vector; vg, viral genomes.

expressing mCherry under the control of the previously described hepatocyte-specific enhanced transthyretin promoter at a dose of $2.5x10^{10}$ transducing units/kg).[34] There was no difference in the percentage of EdU-positive hepatocytes between LV-positive and LV-negative cells during the first week after LV administration, suggesting that proliferation was equally distributed between transduced and untransduced hepatocytes, as assessed by EdU incorporation (Fig. 3G). We measured LV-positive tissue in mice treated as newborns at different times *post*-LV and observed approximately 10% stable gene marking over time, indicating maintenance of the percentage of LV-transduced hepatocytes during liver growth (Fig. 3H). These data show that LV-mediated genetic modification is equally distributed between proliferating and non-proliferating hepatocytes in newborn mice, leading to stable maintenance of the proportion of the genetically modified liver. As expected, the mathematical model confirmed the observed outcome (Fig. 3I,J).

UMAP of single nuclei identified as hepatocytes in (A), showing expression of the *Alb* gene. (G) Violin plot of *Alb* expression in each cluster shown in (B). APC, antigen-presenting cells; GSEA, gene set-enrichment analysis; NES, normalized enrichment score; snRNA-seq, single-nucleus RNA sequencing; UMAP, uniform manifold approximation and projection.

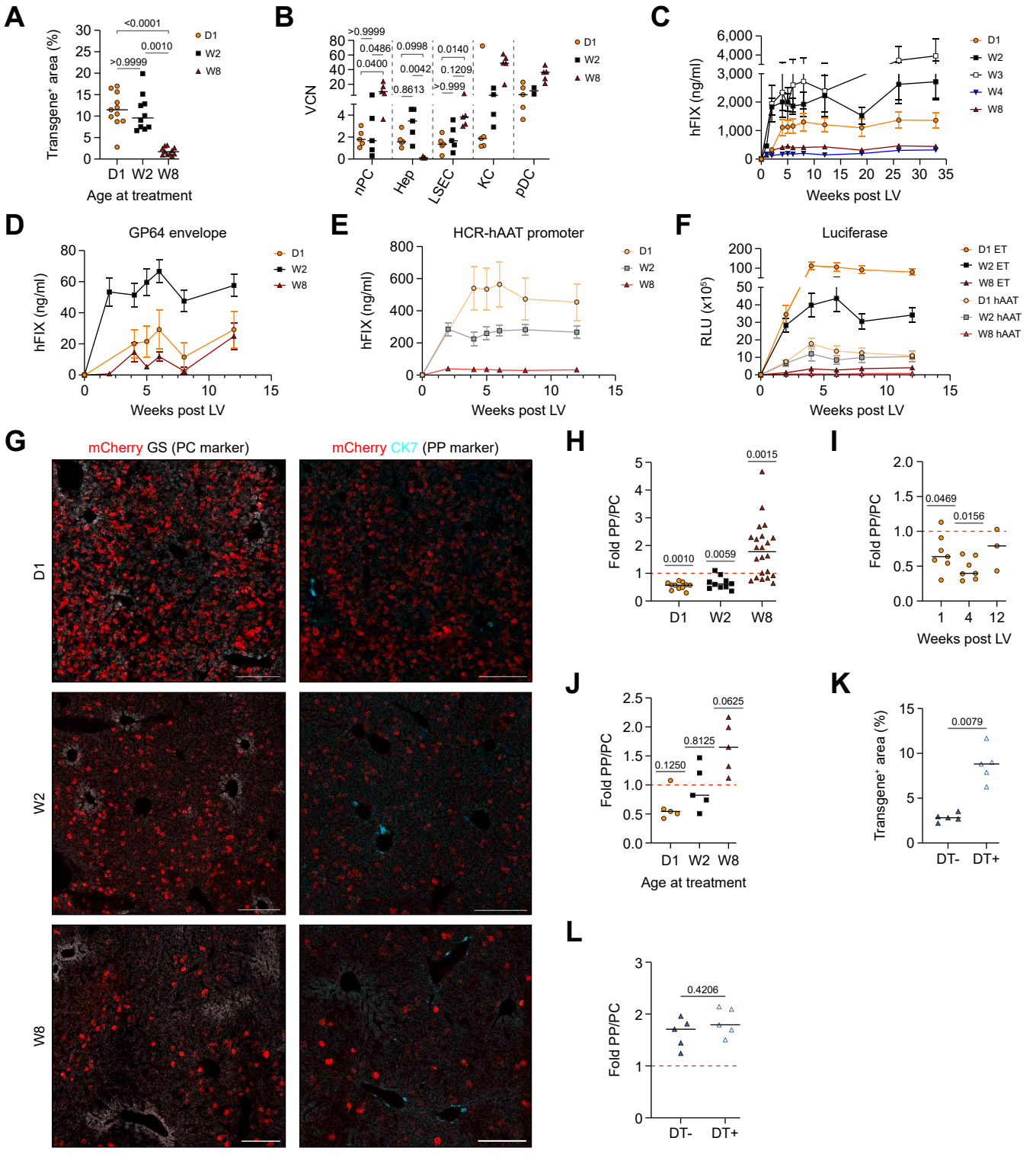

Fig. 4. *In vivo* administration of LV to young mice leads to greater hepatocyte transduction and transgene expression than in adult-treated mice. (A) Single values and median percentages of liver transgene-positive tissue area measured 3-7 days post i.v. administration of an LV ($2.5x10^{10}$ transducing units/kg) expressing a fluorescent reporter (GFP, mCherry, or BFP) in mice treated at specified ages: postnatal day 1 (D1), week 2 (W2), or week 8 (W8). Kruskal-Wallis test with Dunn's multiple comparisons test. D1 n = 11, W2 n = 10, W8 n = 11. (B) Single values and median of VCN measured in NPCs or FACS-sorted hepatocytes (Hep), LSECs, KCs, and pDCs 3 days post i.v. LV administration ($2.5x10^{10}$ transducing units/kg). Kruskal-Wallis test with Dunn's multiple comparisons test. NPCs: D1 n = 5, W2 n = 5, W8 n = 5; Hep: D1 n = 5, W2 n = 5, W8 n = 5; LSECs: D1 n = 5, W2 n = 5, W8 n = 5; KCs: D1 n = 5, W2 n = 4, W8 n = 5; pDCs: D1 n = 5, W2 n = 2, W8 n = 5. (C) Mean ± SEM of hFIX measured in the plasma of mice treated at different ages by i.v. administration of VSV.G-pseudotyped LV expressing hFIX under the ET promoter ($2.5x10^{10}$ transducing units/kg). LME models followed by *post hoc* analysis; comparisons against the W8 group were performed for the last time point. D1 *vs.* W8 $p = 0.0003$, W2 *vs.* W8 $p < 0.0001$, W3 *vs.* W8 $p = 0.0014$, W4 *vs.* W8 $p = 0.6506$. D1 n = 14, W2 n = 13, W3 n = 5, W4 n = 5, W8 n = 15. (D-E) Mean ± SEM of hFIX measured in the plasma of mice treated at various ages by i.v. administration of $2.5x10^{10}$ transducing units/kg of (D) GP64-pseudotyped LV expressing hFIX under the ET promoter

The age of LV administration affects the efficiency and localization of gene transfer within the liver lobule

We next set out to investigate the impact of the age of administration on the efficiency of *in vivo* gene transfer to hepatocytes by LV. We selected three different ages to capture most of the liver growth: D1 (newborn), week 2 (W2, juvenile), which is just before weaning, or week 8±2 (sexually mature, adults). We i.v. administered $2.5x10^{10}$ transducing units/kg of a VSV.G-pseudotyped LV expressing a fluorescent reporter. We found a similar percentage of transgene-positive liver tissue in newborn and juvenile mice, significantly higher (about 4-fold) than in adults, 3-7 days post-LV administration (Fig. 4A). Similar results were obtained when using integrase-defective LV, by modifying the envelope protein (GP64) or changing the hepatocyte-specific promoter driving transgene expression (HCR-hAAT [hepatic control region coupled to alpha-1-antitrypsin]). This suggests that the larger transgene-positive liver area in young compared to adult mice is independent of LV pseudotype, integration, and transgene expression (Fig. S4A–C). We then measured LV copies per diploid genome (vector copy number [VCN]) in different liver cell types: non-parenchymal cells (NPCs), enriched by density gradient, hepatocytes, liver sinusoidal endothelial cells (LSECs), Kupffer cells (KCs), plasmacytoid dendritic cells, purified by FACS, 3 days after LV administration, as previously described.[19] We observed higher VCN in hepatocytes in young mice compared to adult mice, accompanied by lower VCN in NPCs (LSECs, KCs, and plasmacytoid dendritic cells) in the former relative to the latter. However, we did not detect significant differences in VCN among newborn or juvenile mice (Fig. 4B). These data suggest that hepatocytes are more permissive to LV transduction in young mice than in adults, partly due to reduced transduction in liver NPCs. We then utilized a human FIX (hFIX)-expressing LV to monitor transgene output longitudinally and included mice aged 3 to 4 weeks to identify when the decrease in transduction efficiency occurs. We confirmed higher transgene output in newborn and juvenile mice compared to adults, with mice treated at week 4 showing hFIX levels similar to those in adult-treated mice, while mice treated at week 3 exhibited hFIX levels comparable to those treated as juveniles. This suggests that changes occur in the liver around weaning, when liver functions undergo substantial reprogramming (Fig. 4C). Interestingly, juvenile mice showed double the hFIX output compared to newborns, despite the similar transgene-positive liver area observed with fluorescent transgenes. To further explore this aspect, we treated mice of different ages using LV with GP64 as the envelope protein, HCR-hAAT as a hepatocyte-specific promoter or a secreted form of luciferase. While the differences between young and adult mice were consistent across all LV types, differences in transgene output between newborns and juveniles appeared to depend on the promoter and transgene used (Fig. 4D–F), suggesting that different hepatocyte populations may be transduced at these stages of liver growth where certain promoters are expressed and/or transgenes secreted differently. Notably, levels of circulating transgene protein remained stable for up to 8 months following LV administration (the last time analyzed), confirming the stability of transgene output, regardless of the age at treatment. The observed differences were attributed to the age of the mice at the time of LV administration rather than their age at the time of analysis. Additionally, differences in FIX transgene output between mice treated at various ages were confirmed at higher LV doses (Fig. S4D). To assess the safety of LV integration in hepatocytes transduced at different ages, we examined LV genomic integration sites (IS) >8 months after administration in FACS-sorted hepatocytes from mice treated at various ages. There were no dominant clones or enrichment of IS near or within cancer genes, confirming the absence of LV-mediated genotoxicity, regardless of age at administration (Fig. S4E and F).

We then investigated whether LV gene transfer was enriched in different regions of the liver lobule. To this end, we identified the PC zone by immunostaining for glutamine synthetase and the PP zone by immunostaining bile ducts (cytokeratin 7) and segmenting based on specified radii (see supplementary materials and methods section). We observed a higher transgene-positive area in the PC compared to the PP zone in mice treated as newborns or juveniles, while a PP bias was evident in mice treated as adults (Figs. 4G,H and S5A-C). This spatial bias was maintained over time, indicating that it

(D1 n = 4, W2 n = 7, W8 n = 5) or (E) VSV.G-pseudotyped LV expressing hFIX under the HCR-hAAT promoter. LME followed by *post hoc* analysis; pairwise comparisons among groups were performed for the last time point. D1 *vs.* W2 $p = 0.6737$, D1 *vs.* W8 $p < 0.0001$, W2 *vs.* W8 $p = 0.0004$. D1 n = 10, W2 n = 12, W8 n = 10. (F) Mean ± SEM of RLU measured in serum of mice treated at different ages by i.v. administration of VSV.G-pseudotyped LV expressing secreted Gaussia luciferase (Gluc) under the ET or HCR-hAAT promoter, as specified ($2.5x10^{10}$ transducing units/kg). LME followed by *post hoc* analysis; pairwise comparisons among groups were conducted for the last time point. ET: D1 *vs.* W2 $p = 0.0158$, D1 *vs.* W8 $p < 0.0001$, W2 *vs.* W8 $p = 0.0004$; HCR-hAAT D1 *vs.* W2 $p = 1$, D1 *vs.* W8 $p = 0.0147$, W2 *vs.* W8 $p = 0.0231$. ET: D1 n = 5, W2 n = 5, W8 n = 5; HCR-hAAT: D1 n = 5, W2 n = 5, W8 n = 5. (G) Representative images of livers from D1, W2, and W8 mice, as shown in (H), with immunostaining to identify PC area using GS antibody to mark central hepatocytes (left panel) or identification of PP area using CK7 antibody to mark bile ducts (right panel). Scale bar = 200 μm. (H) Single values and median of transgene-positive liver tissue area expressed as a fold change between the percentage of positive PP and PC area (see supplementary materials and methods section), analyzed 3-7 days post i.v. administration of LV ($2.5x10^{10}$ transducing units/kg) expressing a fluorescent reporter in mice treated at D1, W2, or W8. Red dotted line = 1. One-sample Wilcoxon signed-rank test *vs.* 1. D1 n = 11, W2 n = 10, W8 n = 22. (I) Single values and median of transgene-positive liver tissue area expressed as a fold change between the percentage of positive PP and PC area analyzed 1, 4, or 12 weeks post i.v. administration of LV ($1x10^{10}$ transducing units/kg) expressing GFP in newborn mice, measured by IF analysis. Red dotted line = 1. One-sample Wilcoxon signed-rank test *vs.* 1. 1 week n = 7, 4 weeks n = 7, 12 weeks n = 3. (J) Single values and median of transgene-positive liver tissue area expressed as a fold change between the percentage of positive PP and PC area, analyzed 6 weeks post i.v. administration of LV ($2.5x10^{10}$ transducing units/kg) expressing mCherry in mice treated at D1, W2, or W8, measured by IF analysis. Red dotted line = 1. One-sample Wilcoxon signed-rank test vs. 1. D1 n = 5, W2 n = 5, W8 n = 5. (K) Single values and median of liver transgene-positive area measured 7 days post i.v. administration of LV ($2.5x10^{10}$ transducing units/kg) expressing mCherry in *Clec4f-DTR* adult mice with or without DT treatment 12 h prior to LV administration. Mann-Whitney test. DT-n = 5, DT+ n = 5. (L) Single values and median of transgene-positive liver tissue area expressed as a fold change between the percentage of positive PP and PC area of mice in (F), measured by IF analysis. Red dotted line = 1. Mann-Whitney test. BFP, blue fluorescent protein; CK7, cytokeratin 7; DT, diphtheria toxin; GFP, green fluorescent protein; GS, glutamine synthetase; hAAT, human alpha-1 antitrypsin; Hep, hepatocytes; hFIX, human coagulation factor IX; IF, immunofluorescence; KC, Kupffer cell; LME, linear mixed-effects; LV, lentiviral vector; LSECs, liver sinusoidal endothelial cell; NPCs, non-parenchymal cells; pDCs, plasmacytoid dendritic cells; PC, pericentral; PP, periportal; RLU, relative light unit; VCN, vector copy number; VSV.G, vesicular stomatitis virus glycoprotein.

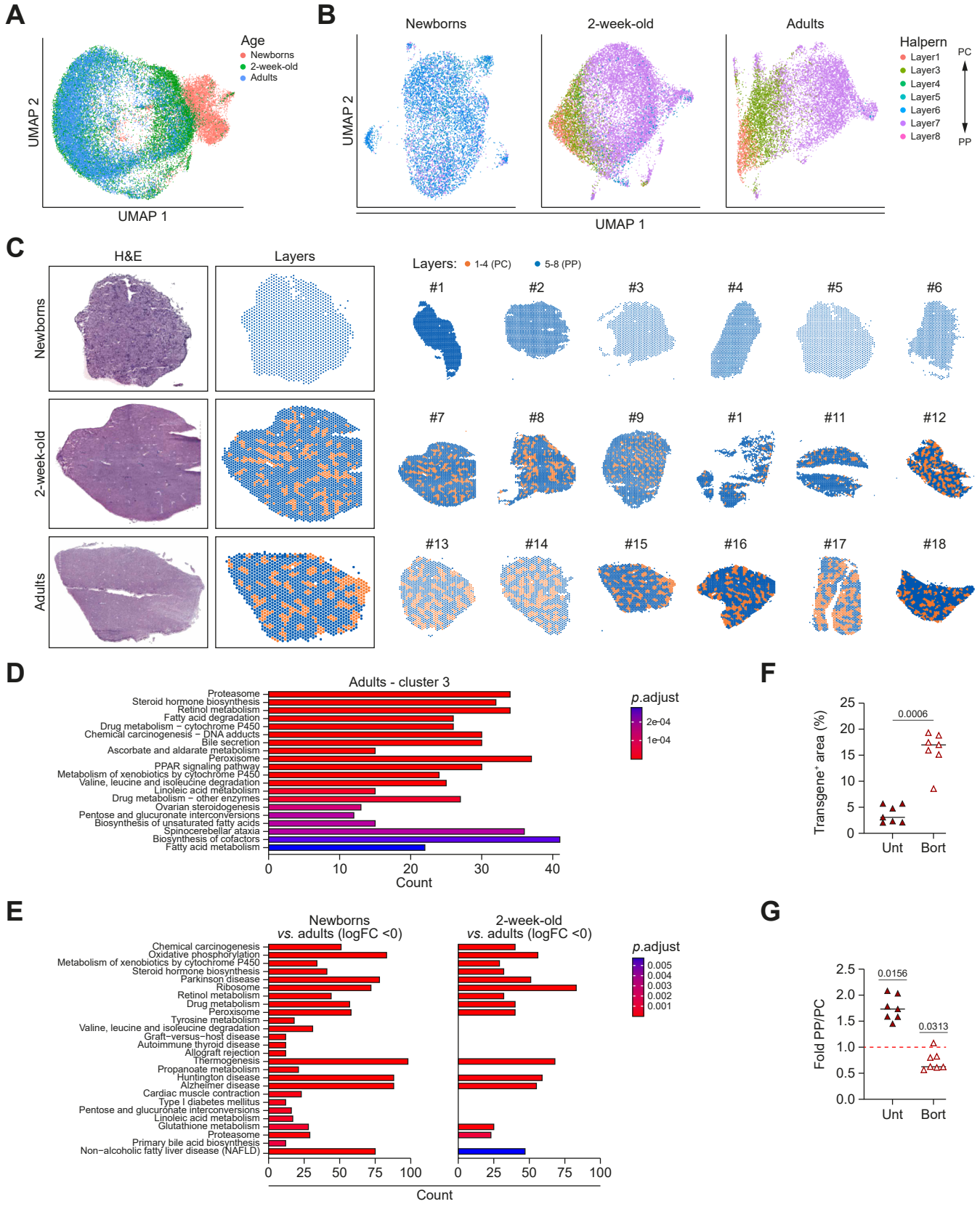

Fig. 5. The zonated hepatocyte transcriptomic profile is established over time. (A) UMAP of liver spots from mice in all groups, color-coded by age. (B) UMAP plot showing liver spots from newborn, 2-week-old, or adult mice, colored based on the transcriptional profile of layers 1-8 from Halpern *et al.*[2] (C) Representative images of H&E staining of livers from newborn, 2-week-old, and adult mice, with spots categorized into layers 1-4 (PC, orange) or layers 5-8 (PP, blue) on their corresponding slices. On the right, the mapping of spots across all liver samples is presented. (D) Bar plot of enriched pathways (adjusted p <0.001) for DEGs that are

resulted from transduction rather than transgene expression (Figs 4I,J and S5D-F). To determine if this outcome depended on the increased capture of LV by KCs in adult mice (see Fig. 4B),[35] we used a mouse line expressing diphtheria toxin receptor (DTR) under a KC-specific marker (*Clec4f-DTR*),[36] allowing KC-specific depletion upon DT administration (Fig. S5G). In *Clec4f-DTR* adult mice treated with DT 12 h before LV, we observed an increase in the transgene-positive area (Fig. 4K), consistent with previous reports;[19] however, LV continued to preferentially transduce the PP zone (Figs. 4L and S5H). Overall, these data show that the efficiency of *in vivo* hepatocyte gene transfer by LV is influenced by age at the time of administration, with the most significant changes noted when LV is given before or after weaning. Furthermore, LV transduction occurred preferentially in the PC zone in young mice and in the PP zone in adult mice, independent of KC involvement.

The transcriptional landscape of zonated hepatocytes is progressively established during growth and impacts LV gene transfer

The extensive evidence of spatiotemporal hepatocyte heterogeneity prompted us to perform longitudinal spatial transcriptomics of liver tissue during physiological growth. We used samples from newborn, juvenile, or adult mice, which were either LV-transduced, 3 days post-LV, or age-matched untransduced mice. In this technique, liver tissue slices are placed onto slides with bar-coded spots, allowing the sequenced RNA to be assigned to a specific position within the tissue.[37] We initially assessed the potential effects of LV transduction on hepatic transcriptomes. We observed more LV-positive spots in the livers of newborn and juvenile mice compared to adults, as evidenced by the presence of LV RNA, confirming a higher level of transduction in the former (Fig. S6A). Furthermore, we confirmed the preferential LV transduction of PP hepatocytes, as indicated by the upregulation of PP genes and the downregulation of PC genes in LV-positive compared to LV-negative spots in adult mice (Fig. S6B). Only a few genes were differentially expressed between LV-positive and LV-negative spots, with none shared among the age groups, indicating minimal changes to the transcriptomic profile due to LV transduction in this context (Fig. S6C–E).

Analyzing the spots across all the samples revealed age-dependent differences in the transcriptomic profile, with the most distinct spots belonging to newborn livers and those of juvenile livers being more similar to adult livers (Fig. 5A). We then mapped the transcriptomic profile of the lobule layers identified in the single-cell RNA-seq study by Halpern *et al.*[2] onto our samples, assigning each spot a similarity score (layers 1-4 PC, layers 5-8 PP). We found that layers characterized by a PC transcriptome were absent in newborns, appeared in juvenile livers, and were fully recognized in adults (Fig. 5B,C), indicating progressive establishment of zonation during postnatal liver growth, consistent with previous reports.[3] By mapping the same layers onto the hepatocyte clusters identified by the snRNA-seq described above (see Fig. 2), we confirmed the exclusive presence of PP layers in newborn hepatocytes (Fig. S7A). Unsupervised clustering of the spots mirrored the zonation indicated by the "Halpern" layers in adult livers, but not in newborn and juvenile livers, confirming well-separated PC and PP transcriptomes only in adults (Fig. S7B). We performed GSEA between different clusters in newborn livers, noting enrichment in cell cycle and proliferation pathways in cluster 1, while cluster 0 was characterized by some hepatocyte-specific functional pathways (Fig. S7C). The same analysis in juvenile livers highlighted an initial establishment of compartmentalization of metabolic activities between clusters (Fig. S7D). Consistently, the expression of known zonated genes was segregated in 2-week-old and adult livers (Fig. S7E). We confirmed the absence of clear zonation in newborn livers for proteins known to be zonated in adult livers by immunohistochemistry staining (Fig. S7F). We then performed snRNA-seq analyses on 2-week-old and 8-week-old livers, confirming the progressive establishment of zonation and decrease in proliferation at single-cell resolution (Fig. S8A–F). Pseudo-time analysis of the entire spatial transcriptomic dataset beginning with the newborn livers demonstrated a progressive evolution from layers with PP-like transcriptomes to those exhibiting a more PC-like identity, further supporting the maturation of zonated phenotypes (Fig. S8G). Interestingly, the same analysis conducted on the snRNA-seq dataset revealed a trajectory starting from the more proliferative and less differentiated hepatocyte clusters, progressing toward the more differentiated ones (Fig. S8H). *Post hoc* analysis of enriched genes in the more PC spots of adult livers (cluster 3, see Fig. S6B) revealed an upregulation of the proteasome pathway, along with other metabolic pathways typical of PC hepatocytes (Fig. 5D). The proteasome pathway was also upregulated in adult liver samples compared to both newborn and juvenile livers (Fig. 5E). Interestingly, the enrichment of the proteasome pathway showed an inverse correlation with permissiveness to LV transduction, as the latter was lower in adult hepatocytes, particularly in the PC area (see Fig. 4). Proteasome inhibitors have been shown to improve LV transduction in stem cells *in vitro*.[38] Consequently, we administered the proteasome inhibitor bortezomib to adult mice prior to LV delivery. We observed a remarkable 4-fold increase in transgene-positive liver area in bortezomib pre-treated mice compared to LV-only controls, with a PC transduction bias (Figs. 5F,G and S8I), suggesting that proteasome activity significantly restricts *in vivo* LV gene transfer

upregulated in cluster 3 from the unsupervised clustering of adult mice (see Fig. S7B). Counts on the X-axis represent the number of enriched genes in each term, while the colors of the bars indicate statistical significance (adjusted p value). (E) Bar plot of enriched pathways (adjusted p <0.001) for DEGs that are downregulated in newborn and 2-week-old mice compared to adult mice. (F) Single values and median of the liver transgene-positive area measured 2 weeks after i.v. administration of an LV ($2.5x10^{10}$ transducing units/kg) expressing mCherry in adult mice treated with (Bort) or without (Unt) i.v. administration of two doses of bortezomib (1 mg/kg each), given 12 and 1 h prior to LV administration. Mann-Whitney test. Unt n = 7, Bort n = 7. (G) Single values and median of transgene-positive liver tissue area presented as the fold difference between the percentages of positive PP and PC areas in mice from (E). One-sample Wilcoxon signed-rank test *vs*. 1. The red dotted line indicates 1. DEGs, differentially expressed genes; LV, lentiviral vector; PC, pericentral; PP, periportal; Unt, untreated; UMAP, uniform manifold approximation and projection.

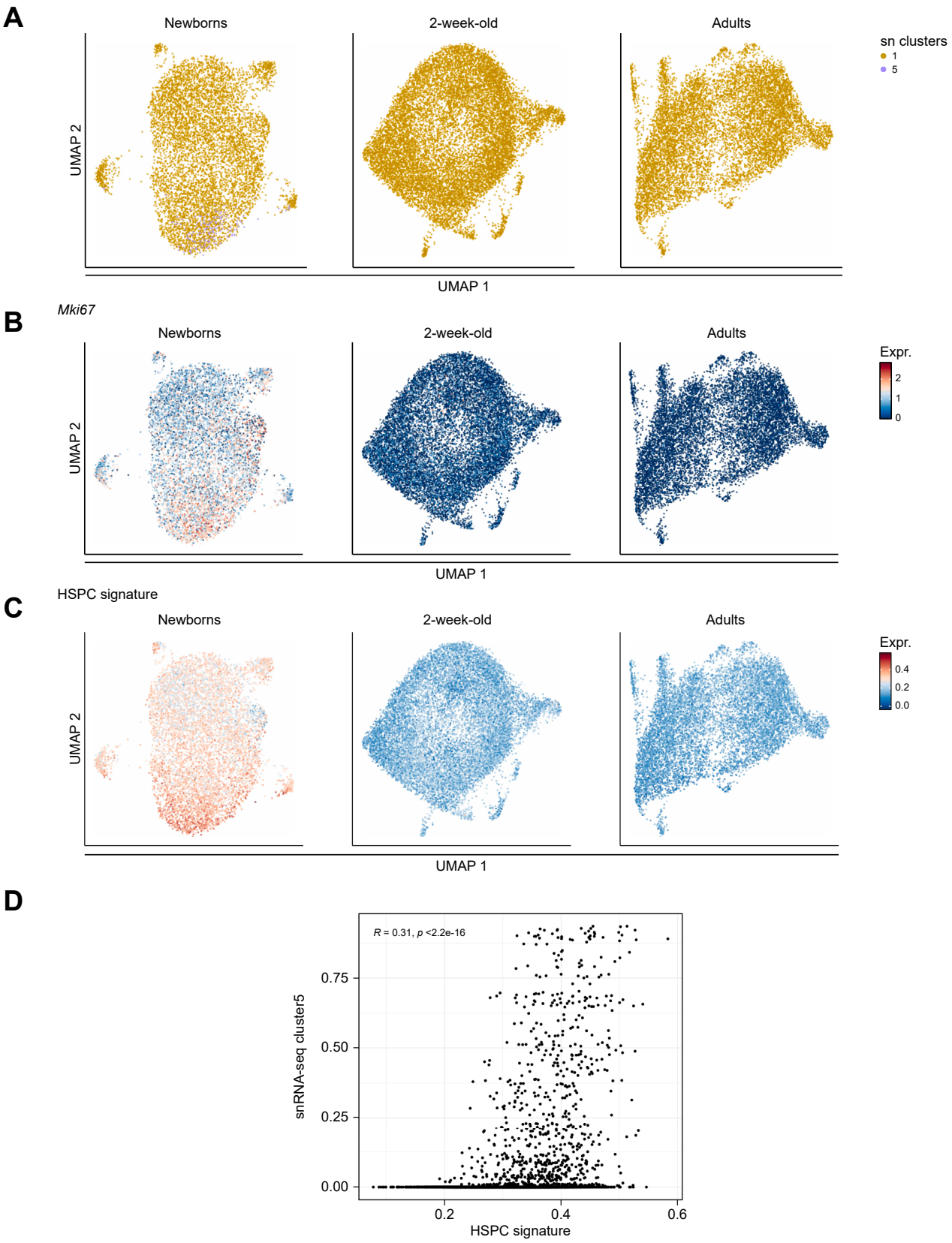

Fig. 6. Proliferating hepatocytes colocalize with HSPCs in the newborn liver. (A) UMAP of liver spots from newborns, 2-week-old, or adult mice color-coded according to similarity to clusters identified by snRNA-seq in newborn livers (see Fig. 2). Cluster 5, which contains proliferating hepatocytes, is found only in newborns, whereas more differentiated hepatocytes identified by cluster 1 are present across all ages. (B,C) UMAP of liver spots from newborns, 2-week-old, or adult mice showing the expression of the *Mki67* gene (B) and the expression of the HSPC signature (C). (D) Scatter plot of spots from newborn livers illustrating the

to hepatocytes, especially in the PC zone. Overall, these data show that the newborn liver displays a PP-like transcriptional landscape and that the PC identity, which emerges in hepatocytes around weaning, is linked to lower permissiveness for *in vivo* LV gene transfer.

Finally, we analyzed the transcriptome of LSECs at different ages. LSECs represent another potential target for liver gene therapy strategies, as they produce, for instance, coagulation factor VIII and von Willebrand Factor, whose mutations lead to hemophilia A and von Willebrand disease, respectively. We observed a similar cluster composition after unbiased subclustering of snRNA-seq datasets across different ages (Fig. S8J and K). We examined *Mki67* expression and found that proliferating LSECs were enriched in cluster 2 (Fig. S8L). Like hepatocytes, proliferating LSECs were more abundant in newborn livers, and nearly absent in adult livers (Fig. S8M). These data suggest that, even for gene therapy strategies targeting LSECs, it would be important to genetically engineer the proliferating cells to stably maintain the therapeutic transgene during physiological liver growth.

Clonogenic hepatocytes are located near hematopoietic cells in a spatial niche in the newborn liver

We subsequently mapped the transcriptional profile of all the identified hepatocyte clusters from the newborn snRNA-seq (see Fig. 2) onto the spatial transcriptomic dataset. We found that the transcriptome of the more differentiated hepatocyte cluster (cluster 1) was prevalent in juvenile and adult livers, whereas the transcriptome of the more replicative hepatocyte subset (cluster 5) was enriched in some of the spots of the newborn livers (Fig. 6A). We also mapped the expression of *Mki67* to identify spots with actively replicating cells. We observed a progressively decreasing intensity of expression (Fig. 6B), consistent with the reduced proliferation rate noted from EdU administration at these ages (see Fig. 1F). Furthermore, we mapped an HSPC signature onto the spatial transcriptomic dataset and identified high expression in several spots of the newborn liver, confirming ongoing hematopoiesis (Fig. 6C). Interestingly, the transcriptional profile of cluster 5 was elevated in some of the spots enriched with the HSPC signature (Fig. 6D), suggesting co-localization of the more proliferative hepatocytes with highly cycling HSPCs. This finding correlated well with the previous observation that replicating hepatocytes are characterized by high expression of genes related to heme metabolism (see Fig. 2E), suggesting their proximity to erythropoietic islands. These data suggest the presence of a local hub consisting of clonogenic hepatocytes and HSPCs.

To further explore this aspect, we performed a distinct spatial transcriptomic analysis of a newborn liver, employing multiplexed error-robust fluorescence *in situ* hybridization (MERFISH), a high-resolution *in situ* transcriptomic imaging technique.[39] We then mapped the signatures of the various cell types identified in the snRNA-seq data onto the MERFISH dataset and found cells corresponding to the identified cell populations, including HSPCs, endothelial cells, and antigen-presenting cells (APCs: likely KC-like cells; Fig. 7A). Most of the cells (85%) were classified as hepatocytes, which was expected due to their larger size and abundant RNA; we also identified the more proliferating subset of hepatocytes (cluster 5). We performed a neighborhood analysis, which further confirmed the proximity of cluster 5 hepatocytes to the HSPCs (Fig. 7B). To identify potential signals regulating gene expression in cluster 5 hepatocytes, we performed a Nichenet analysis on the snRNA-seq dataset,[40] designating cluster 5 among hepatocytes as receivers and selecting various cell types as potential senders (HSPCs, hepatocytes, APCs, fibroblasts, or endothelial cells). We identified 28 candidate ligands that could be responsible for the transcriptional program of clonogenic hepatocytes, highlighting *Bmp2, Lama2, Fgf1, Igf1, Igf2,* and *Il15* as those with the highest regulatory potential (Fig. 7C). Fibroblast growth factor 1 (FGF1), insulin-like growth factor (IGF) 1 and 2 are growth factors previously linked to hepatocyte proliferation in the context of regeneration.[41–43] BMP2 (bone morphogenetic protein 2) acts as a developmental signal that also induces hepatic fate decisions[44] and functions as an LSEC-derived angiocrine signal involved in iron homeostasis.[45] Laminin subunit alpha 2 is an extracellular matrix protein present in the LSEC basement membrane that also plays a role in inducing cell proliferation.[46] IL-15 has been previously associated with liver regeneration.[47] We then analyzed where these genes were primarily expressed and found that a subset of endothelial cells, fibroblasts, APCs, and hepatocytes themselves expressed these genes at high levels (Fig. 7D). Consistent with our neighborhood analysis, we identified regions where these cells are localized near HSPCs and cluster 5 hepatocytes in the MERFISH analysis (Fig. 7E). We also stratified HSPCs based on *Mki67* expression and conducted Nichenet analysis, designating the two most proliferative HSPC clusters as receivers and the other cell types as senders (Fig. S9A–D). Interestingly, *Fgf1* and *Igf1* were identified among the candidate ligands that regulate this transcriptional program (Fig. S9E). We then confirmed by immunohistochemistry the close proximity of proliferating hepatocytes, identified as Ki67-positive, and hematopoietic islands in newborn livers (Fig. 8A).

To experimentally confirm the hits identified by Nichenet analysis as potential signals guiding the transcriptional program of cluster 5 hepatocytes, we cultured primary newborn hepatocytes for 48 h in the presence or absence of BMP2, FGF1, IGF1, IGF2, and IL-15. We then analyzed differentially expressed genes between stimulated and unstimulated hepatocytes and mapped the top 100 upregulated genes from the former onto the newborn snRNA-seq dataset. Stimulation with this cocktail of molecules induced the upregulation of genes highly enriched in cluster 5, thereby confirming a role for these signals in shaping the transcriptional program of cluster 5 hepatocytes (Fig. 8B,C). Importantly, among the upregulated genes in stimulated hepatocytes, we identified genes involved in the "Wnt" pathway, which is known to support hepatocyte proliferation,[48] as well as *Hamp*, a gene involved in maintaining iron homeostasis, linking back to the heme-metabolism

relationship between the expression of the HSPC signature shown in (C) and the signature of snRNA-seq cluster 5. Pearson correlation coefficient. HSPC, hematopoietic stem and progenitor cell; snRNA-seq, single-nucleus RNA sequencing; UMAP, uniform manifold approximation and projection.

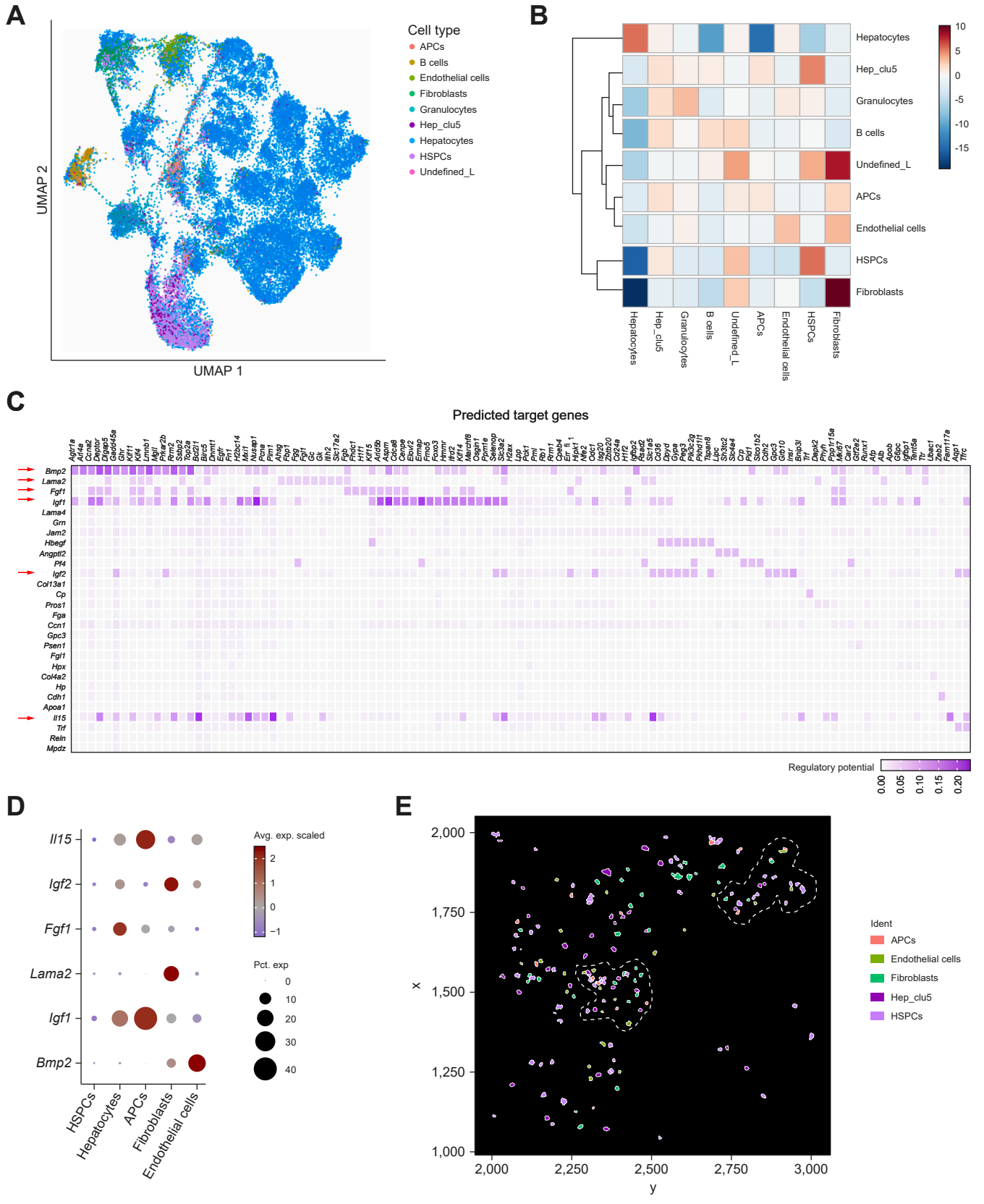

Fig. 7. A spatial niche supports the proliferation of clonogenic hepatocytes and HSPCs. (A) UMAP plot of MERFISH from two slices of a newborn liver, color-coded according to similarity to cell types/clusters identified by snRNA-seq (see Fig. 2). (B) Neighborhood analysis performed on one of the two MERFISH slides, showing a proximity score for the specified cell types/clusters. The asymmetrical matrix should be read row by row, with positive values indicating spatial proximity. (C) Nichenet analysis conducted on the snRNA-seq, using cluster 5 hepatocytes as receivers while selecting cell types as senders (HSPCs, hepatocytes, APCs,

pathway identified in cluster 5 hepatocytes (see Figs 2E and 8D). Overall, these data suggest that various cells collaborate within a spatial niche to instruct the clonogenic phenotype in a subset of hepatocytes, sharing some pro-proliferative signals with HSPCs.

Discussion

Herein, we present an in-depth characterization of the spatiotemporal transcriptional and proliferative heterogeneity of hepatocytes during liver growth, and its impact on the efficiency and long-term stability of *in vivo* hepatocyte genetic engineering – achieved through either LV gene transfer or targeted genome editing, both serving as representative stable genetic modification strategies. We report a lack of evident zonation in the newborn liver and a predominant PP transcriptional profile. The progressive emergence of hepatocytes with a PC-specific transcriptional landscape during growth aligns with the increasing demand for xenobiotic metabolism, coinciding with the transition from breast milk to external feeding, consistent with previous reports.[3] PC hepatocytes exhibit high expression of proteasome pathway genes, which negatively affects the efficiency of *in vivo* LV-mediated gene delivery and contributes to its non-homogeneous lobule distribution. Indeed, proteasome inhibition enhanced the efficiency of hepatocyte gene transfer in adult mice to levels comparable to those in younger mice and eliminated the PP transduction bias. Multiple factors likely contribute to the higher efficiency of *in vivo* LV gene transfer to hepatocytes in mice treated as newborns or juveniles, encompassing both cell-autonomous and non-cell-autonomous influences: high expression of proteasome pathway genes in hepatocytes correlates with low permissiveness to LV transduction, consistent with previous reports on other cell types;[49] additionally, the lower number of LV copies in KCs and LSECs in young mice compared to adults suggests that these NPCs also play a role. The acquisition of a mature KC phenotype, characterized by increased phagocytic activity, has previously been shown to occur during liver growth.[35] Notably, these changes in liver cell types occur after weaning, coinciding with the significant decrease in gene transfer efficiency observed after the third week of life in mice. Other factors may also influence the age-dependent differences in the efficiency of hepatocyte transduction by LV, including those affecting various transduction steps or differing extents of inflammatory/antiviral responses. Our data confirm and expand upon previous reports, also showing higher LV-mediated transgene expression in juvenile mice compared to adults.[20,50] The age at LV administration also impacted the distribution of LV gene transfer within the liver lobule. However, the preferential transduction of PP hepatocytes in adult mice was not due to differential KC phagocytosis, but rather due to an intrinsic feature of PC hepatocytes, which is less pronounced before weaning. Conversely, the preferential transduction of the PC zone in young mice could be attributed to anatomical factors that facilitate LV access to this area. Indeed, it has been shown that egress of liver HSPCs occurs from the PC area, likely implying easier access to the circulation.[51]

The persistence of hematopoietic niches in the newborn liver may create an environment where pro-proliferative signals are locally shared between HSPCs and clonogenic hepatocytes, as highlighted by combining single-cell and spatially resolved transcriptomic analyses. Active heme metabolism by the subset of proliferating hepatocytes near erythropoietic islands may exert a protective role against potential oxidative stress caused by free heme in the local tissue environment.[52,53] Recent reports have also suggested that hepatocytes play a protective role toward HSPCs in the fetal liver.[54] The proximity to these HSPC niches may induce the clonogenic phenotype in some of the newborn hepatocytes. *Ex vivo* induction of all newborn hepatocytes to express a transcriptional profile resembling that of the proliferating subset *in vivo* – stimulated by key signaling molecules selected based on transcriptomic data – supports the idea that local cues shape hepatocellular proliferative heterogeneity within an instructive tissue niche. This niche is composed of distinct NPCs, likely shared with hematopoietic progenitors, in neonatal mouse livers.

We estimate that approximately 15-20% of clonogenic hepatocytes in the newborn liver proliferate and give rise to most of the adult liver, suggesting a gradual reduction in tissue clonality. We propose that clonogenic hepatocytes transmit this feature to daughter cells that proliferate locally at a progressively slower rate throughout organ growth until adulthood. In contrast, the remaining hepatocytes mostly stay quiescent. As a result, we observe a gradual decline in proliferation pathways over time, alongside an increase in pathways associated with mature hepatocyte functions. Further molecular characterization of the clonogenic hepatocyte subset requires additional investigation. Moreover, it remains to be determined whether and how a disease state affects hepatocyte proliferation and maturation during liver growth. We propose a simple mathematical model of hepatocyte proliferation during liver growth that reproduces the experimental data characterizing liver growth dynamics, further supporting our proposed mechanism of liver growth. This mathematical model can be interrogated to predict changes in the genetically engineered liver area over time, based on the initial efficiency of the genetic modification between the proliferating *vs.* quiescent hepatocyte subsets. As it is based on murine data, the predictive value of the current model is limited to the murine lifespan and the low hepatocyte turnover in adulthood. Therefore, further refinement is needed to improve its applicability to human outcomes. HDR-mediated gene editing preferentially occurred in proliferating hepatocytes in newborn mice, resulting in an increased proportion of the gene-edited tissue area, as predicted by the mathematical model. HDR is known to be more active in proliferating cells,[55] likely explaining this preferential editing, although we cannot rule out the possibility of preferential transduction of

fibroblasts, or endothelial cells). (D) Dot plot depicting the expression of the specified genes (identified in panel C as having the highest regulatory potential) in the listed cell types. (E) Representative visualization of the designated cell types in the MERFISH analysis. Hepatocytes, B cells, granulocytes, and undefined cells have been omitted from the visualization for clarity. APC, antigen-presenting cell; HSPC, hematopoietic stem and progenitor cell; MERFISH, multiplexed error-robust fluorescence in situ hybridization; snRNA-seq, single-nucleus RNA sequencing; UMAP, uniform manifold approximation and projection.

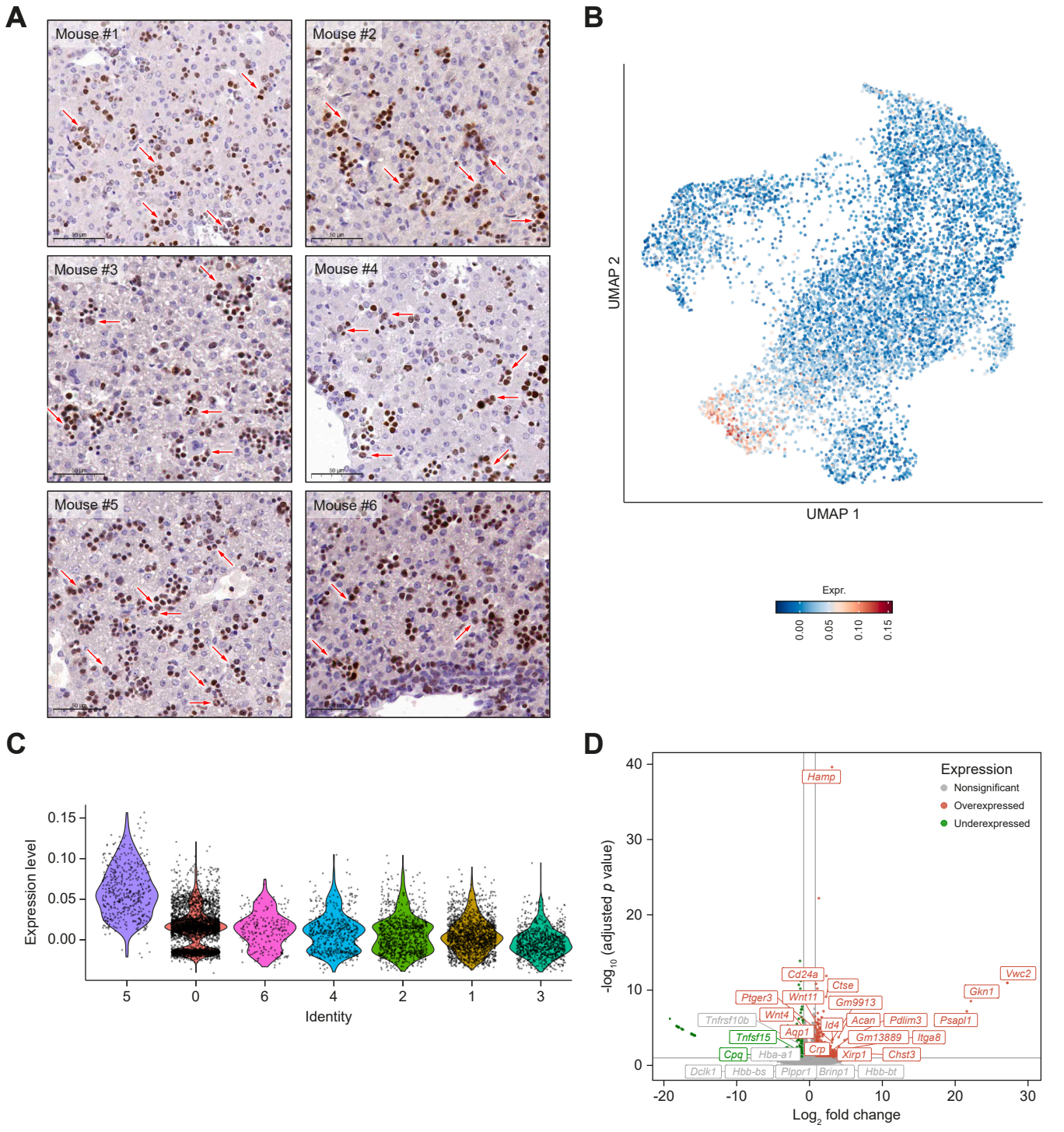

Fig. 8. *Ex vivo* stimulation of newborn hepatocytes with BMP2, IGF1, IGF2, FGF1, and IL15 induces a transcriptional profile similar to that of clonogenic hepatocytes. (A) Representative immunohistochemistry images from newborn mouse livers (n = 6) labeled with anti-Ki67 (brown signal) showing proliferating hepatocytes (red arrows) in close proximity to hematopoietic islands. Scale bar: 50 μm. (B) UMAP of snRNA-seq identified as hepatocytes in Fig. 2A, displaying the expression of the top 100 differentially overexpressed genes (Top 100 DEGs) in *ex vivo*-stimulated newborn hepatocytes compared to unstimulated controls (48 h, cultured with BMP2, IGF1, IGF2, FGF1, and IL15, n = 3 hepatocyte donors). (C) Violin plot of the Top 100 DEGs in each cluster shown in Fig. 2B. (D) Volcano plot of DEGs in *ex vivo*-stimulated newborn hepatocytes compared to unstimulated controls (48 h, cultured with BMP2, IGF1, IGF2, FGF1, and IL15, n = 3 hepatocyte donors). DEG, differentially expressed gene; snRNA-seq, single-nucleus RNA sequencing; UMAP, uniform manifold approximation and projection.

proliferating hepatocytes by AAV vectors as well. Our results emphasize that this genetic modification strategy, if implemented in newborn mice, enables an expansion of the proportion of the genetically modified tissue area by leveraging a physiological mechanism of tissue growth. This suggests that selectively targeting the proliferating subset of hepatocytes may lead to extensive gene modification of the adult liver, yielding an improved therapeutic effect even with an initially lower input of gene marking. Conversely, LV gene transfer was uniformly distributed between the proliferating and quiescent hepatocytes, thus resulting in stable maintenance of the proportion of the LV-transduced liver area over time. Previous reports showed that *in vivo* LV transduction of hepatocytes in adult mice is increased by pre-stimulation with phenobarbital and cholic acid,[56] however, this occurs in a different experimental context than the physiological hepatocyte proliferation observed during liver growth, as examined in the present study. LV transduction did not significantly alter the transcriptomic profile or proliferative capacity of transduced hepatocytes. Consistently, analysis of LV genomic IS showed no expansions of IS near cancer-related genes, regardless of the age at administration. These data confirm earlier studies reporting the absence of liver genotoxicity by LV in both mice and non-human primates.[19,34] Long-term analysis of mice treated at different ages during postnatal liver growth up to adulthood demonstrated stability of transgene expression irrespective of the age of LV delivery. The maintenance of LV-marked hepatocytes with a preferential PP distribution in adult mice during liver turnover suggests that tissue homeostasis is broadly supported by hepatocytes across the lobule.[7,9] Altogether, our work reinforces the concept that the long-term persistence of neonatal gene therapy relies on efficient and harmless genetic modification of both the cell populations responsible for growth and homeostatic turnover in adulthood.

Overall, we provide new insights into the spatiotemporal dynamics of the liver during postnatal growth, highlighting both proliferative and transcriptomic heterogeneity among hepatocytes, the progressive establishment of zonated hepatocyte identity, and their impact on the efficiency and distribution of *in vivo* LV-mediated gene delivery and gene editing. By understanding the biological processes underlying these differences, we were able to manipulate them to enhance outcomes, as demonstrated by proteasome inhibition effectively re-establishing the LV transduction efficiency in adults to levels previously obtained in young mice. We report that not all hepatocytes contribute equally to liver growth, indicating that efficient targeting of clonogenic hepatocytes in the newborn liver is necessary for the long-term maintenance of therapeutic genetic modifications, as shown in the context of LV-mediated gene transfer. Furthermore, this phenomenon can be harnessed to expand the pool of genetically corrected cells, exemplified here by HDR-mediated gene editing. Finally, we reveal the existence of a spatial niche that supports the proliferation of both clonogenic hepatocytes and HSPCs. Gaining a deeper understanding of this niche and its signals may be beneficial for regenerative purposes. This study illuminates the mechanisms of postnatal liver growth and the heterogeneity of hepatocyte subsets, with broad implications for liver biology and therapeutic applications.

Affiliations

[1]*San Raffaele Telethon Institute for Gene Therapy, IRCCS San Raffaele Scientific Institute, Milan, Italy;* [2]*Vita Salute San Raffaele University, Milan, Italy;* [3]*IRCCS San Raffaele Scientific Institute, Milan, Italy;* [4]*ICGEB, Trieste, Italy;* [5]*Institute for Biomedical Technologies, National Research Council, Milan, Italy*

Abbreviations

AAV, adeno-associated virus; DTR, diphtheria toxin receptor; EdU, 5-ethynyl-2′-deoxyuridine; FGF1, fibroblast growth factor 1; GSEA, gene set-enrichment analysis; HDR, homology-directed repair; hFIX, human factor IX; HSPCs, hematopoietic stem/progenitor cells; IGF, insulin-like growth factor; KC, Kupffer cells; LSECs, liver sinusoidal endothelial cells; LV, lentiviral vector; MERFISH, multiplexed error-robust fluorescence *in situ* hybridization; NPCs, non-parenchymal cells; PC, peri-central; PP: peri-portal; snRNA-seq, single-nuclei RNA sequencing; VCN, vector copy number; WT, wild-type.

Financial support

This work was supported by the Fondazione Telethon SR-Tiget Core Grant (TTACC0422TT to A.C.), the Italian Ministry of Health "Giovani Ricercatori" GR-2019-12368956 to F.M. and A.C., and the EU Horizon 2020 Program (825825 UPGRADE). F.St. conducted this study in partial fulfillment of his International Ph.D. Course in Molecular Medicine at San Raffaele University, Milan. M.I. is supported by the European Research Council (ERC) Advanced Grant 101141363, ERC Proof of Concept Grant 101138728, Italian Association for Cancer Research (AIRC) Grants 19891 and 22737, Italian Ministry for University and Research Grants PE00000007 (INF-ACT) and PRIN 2022FMESXL, Funded Research Agreement from Asher Biotherapeutics, VIR Biotechnology, BlueJay Therapeutics.

Conflict of interest

A.C. and C.C. are listed as inventors on a patent application owned by Fondazione Telethon and the San Raffaele Scientific Institute for technology related to this work. Through SR-Tiget, Fondazione Telethon and the San Raffaele Scientific Institute have established a research collaboration with GeneSpire focused on liver-directed lentiviral gene therapy for inherited diseases. A.C. is a co-founder and consultant for GeneSpire. M.I. participates in advisory boards and consultancy roles and receives funding from Gilead Sciences, GentiBio, BlueJay Therapeutics, BioNTech, Excision BioTherapeutics, Moderna, GSK, and Curie. Bio. The remaining authors declare that they have no competing financial interests.

Please refer to the accompanying ICMJE disclosure forms for further details.

Authors' contributions

M.Mi. and F.St. designed and performed experiments, analyzed and interpreted data, and wrote the manuscript. S.B. and M.Mo. performed bioinformatic analyses. C.C., F.Ma., and C.S. performed experiments and analyzed data. S.Z. and D.M. generated the mathematical model and performed the simulations. A.F., F. R. M.B. provided crucial technical support to experiments. E.C. performed image analysis. M.V. performed LV IS analysis and analyzed data. G.B. and A.M. provided crucial reagents, intellectual input, and edited the manuscript. M.G. and R. O. provided crucial support for the MERFISH analysis. F.Sa. and S.D'I. performed histology analyses. E.M. supervised LV IS analyses. F.Mo. and M.I. provided crucial mouse models, reagents, and intellectual input. I.M. supervised bioinformatic analyses. A.C. supervised and coordinated the work, interpreted data, and wrote the manuscript.

Data availability

The LV and reagents described in this manuscript are available to interested scientists upon signing an MTA with standard provisions. All data associated with this study are available in the main text or the "Supplementary materials". RNA-seq and spatial transcriptomics data are deposited in GEO (Accession number GSE236425, GSE274042, GSE296287). The script for all the

bioinformatic analyses (snRNA-Seq and spatial transcriptomic) and for image analysis (zonation) are freely available at http://www.bioinfotiget.it/gitlab/custom/cantore_liverdynamics2023.

Acknowledgements

The Authors wish to thank the Flow cytometry Resource, Advanced Cytometry Technical Applications Laboratory (FRACTAL) and Advanced Light and Electron Microscopy BioImaging Center (ALEMBIC), Center of experimental imaging (CIS), core facilities of IRCCS San Raffaele Scientific Institute; the San Raffaele University Center for Statistics in the Biomedical Sciences (CUSSB) for statistical consultancy; the San Raffaele Center for Omics Sciences (COSR); Martina Rocchi and Rossana Norata for technical support to histology analysis; Lorena Zentilin for AAV stocks preparation at the AAV vector unit of the ICGEB; The Cantore's laboratory for useful discussion; Luigi Naldini for critical reading of the manuscript and helpful discussion.

Supplementary data

Supplementary data to this article can be found online at https://doi.org/10.1016/j.jhep.2025.06.018.

References

Author names in bold designate shared co-first authorship

[1] Jungermann K. Metabolic zonation of liver parenchyma. Semin Liver Dis 1988;8:329–341.
[2] **Halpern KB**, **Shenhav R**, Matcovitch-Natan O, et al. Single-cell spatial reconstruction reveals global division of labour in the mammalian liver. Nature 2017;542:352–356.
[3] **Yang L**, **Wang X**, Zheng JX, et al. Determination of key events in mouse hepatocyte maturation at the single-cell level. Dev Cell 2023;58:1996–2010 e1996.
[4] **Gribben C**, **Galanakis V**, Calderwood A, et al. Acquisition of epithelial plasticity in human chronic liver disease. Nature 2024;630:166–173.
[5] Heinke P, Rost F, Rode J, et al. Diploid hepatocytes drive physiological liver renewal in adult humans. Cell Syst 2022;13:499–507 e412.
[6] Lin S, Nascimento EM, Gajera CR, et al. Distributed hepatocytes expressing telomerase repopulate the liver in homeostasis and injury. Nature 2018;556:244–248.
[7] Chen F, Jimenez RJ, Sharma K, et al. Broad distribution of hepatocyte proliferation in liver homeostasis and regeneration. Cell Stem Cell 2020;26:27–33 e24.
[8] Wei Y, Wang YG, Jia Y, et al. Liver homeostasis is maintained by midlobular zone 2 hepatocytes. Science 2021;371.
[9] **He L**, **Pu W**, **Liu X**, et al. Proliferation tracing reveals regional hepatocyte generation in liver homeostasis and repair. Science 2021;371.
[10] Font-Burgada J, Shalapour S, Ramaswamy S, et al. Hybrid periportal hepatocytes regenerate the injured liver without giving rise to cancer. Cell 2015;162:766–779.
[11] **Huch M**, **Gehart H**, van Boxtel R, et al. Long-term culture of genome-stable bipotent stem cells from adult human liver. Cell 2015;160:299–312.
[12] Campana L, Esser H, Huch M, et al. Liver regeneration and inflammation: from fundamental science to clinical applications. Nat Rev Mol Cell Biol 2021;9:608–624.
[13] **Xu J**, **Guo P**, **Hao S**, et al. A spatiotemporal atlas of mouse liver homeostasis and regeneration. Nat Genet 2024;56:953–969.
[14] Milani M, Starinieri F, Fabiano A, et al. Identification of hepatocyte-primed cholangiocytes in the homeostatic liver by in vivo lentiviral gene transfer to mice and non-human primates. Cell Rep 2025;44:115341.
[15] Puzzo F, Kay MA. The deLIVERed promises of gene therapy: past, present, and future of liver-directed gene therapy. Mol Ther 2025;5:1966–1987.
[16] Pipe SW, Leebeek FWG, Recht M, et al. Gene therapy with etranacogene dezaparvovec for hemophilia B. N Engl J Med 2023;388:706–718.
[17] Mahlangu J, Kaczmarek R, von Drygalski A, et al. Two-year outcomes of valoctocogene roxaparvovec therapy for hemophilia A. N Engl J Med 2023;388:694–705.
[18] Clar J, Mutel E, Gri B, et al. Hepatic lentiviral gene transfer prevents the long-term onset of hepatic tumours of glycogen storage disease type 1a in mice. Hum Mol Genet 2015;24:2287–2296.
[19] **Milani M**, **Annoni A**, Moalli F, et al. Phagocytosis-shielded lentiviral vectors improve liver gene therapy in nonhuman primates. Sci Transl Med 2019;11.
[20] Milani M, Canepari C, Liu T, et al. Liver-directed lentiviral gene therapy corrects hemophilia A mice and achieves normal-range factor VIII activity in non-human primates. Nat Commun 2022;13:2454.
[21] Nicolas CT, VanLith CJ, Hickey RD, et al. In vivo lentiviral vector gene therapy to cure hereditary tyrosinemia type 1 and prevent development of precancerous and cancerous lesions. Nat Commun 2022;13:5012.
[22] Milani M, Canepari C, Assanelli S, et al. GP64-pseudotyped lentiviral vectors target liver endothelial cells and correct hemophilia A mice. EMBO Mol Med 2024;16:1427–1450.
[23] **Anzalone AV**, **Koblan LW**, Liu DR. Genome editing with CRISPR-Cas nucleases, base editors, transposases and prime editors. Nat Biotechnol 2020;38:824–844.
[24] Yin H, Song CQ, Dorkin JR, et al. Therapeutic genome editing by combined viral and non-viral delivery of CRISPR system components in vivo. Nat Biotechnol 2016;34:328–333.
[25] **Wang L**, **Yang Y**, Breton CA, et al. CRISPR/Cas9-mediated in vivo gene targeting corrects hemostasis in newborn and adult factor IX-knockout mice. Blood 2019;133:2745–2752.
[26] De Caneva A, Porro F, Bortolussi G, et al. Coupling AAV-mediated promoterless gene targeting to SaCas9 nuclease to efficiently correct liver metabolic diseases. JCI Insight 2019;5.
[27] **Tornabene P**, **Ferla R**, **Llado-Santaeularia M**, et al. Therapeutic homology-independent targeted integration in retina and liver. Nat Commun 2022;13:1963.
[28] **Bock D**, **Rothgangl T**, **Villiger L**, et al. In vivo prime editing of a metabolic liver disease in mice. Sci Transl Med 2022;14:eabl9238.
[29] Snippert HJ, van der Flier LG, Sato T, et al. Intestinal crypt homeostasis results from neutral competition between symmetrically dividing Lgr5 stem cells. Cell 2010;143:134–144.
[30] Strogatz SH. Nonlinear dynamics and chaos. 2018.
[31] Furchtgott LA, Chow CC, Periwal V. A model of liver regeneration. Biophys J 2009;96:3926–3935.
[32] Sohlenius-Sternbeck AK. Determination of the hepatocellularity number for human, dog, rabbit, rat and mouse livers from protein concentration measurements. Toxicol In Vitro 2006;20:1582–1586.
[33] Barzel A, Paulk NK, Shi Y, et al. Promoterless gene targeting without nucleases ameliorates haemophilia B in mice. Nature 2015;517:360–364.
[34] **Cantore A**, **Ranzani M**, Bartholomae CC, et al. Liver-directed lentiviral gene therapy in a dog model of hemophilia B. Sci Transl Med 2015;7:277ra228.
[35] Gola A, Dorrington MG, Speranza E, et al. Commensal-driven immune zonation of the liver promotes host defence. Nature 2021;589:131–136.
[36] Scott CL, Zheng F, De Baetselier P, et al. Bone marrow-derived monocytes give rise to self-renewing and fully differentiated Kupffer cells. Nat Commun 2016;7:10321.
[37] **Stahl PL**, **Salmen F**, Vickovic S, et al. Visualization and analysis of gene expression in tissue sections by spatial transcriptomics. Science 2016;353:78–82.
[38] Santoni de Sio FR, Cascio P, Zingale A, et al. Proteasome activity restricts lentiviral gene transfer into hematopoietic stem cells and is down-regulated by cytokines that enhance transduction. Blood 2006;107:4257–4265.
[39] **Chen KH**, **Boettiger AN**, **Moffitt JR**, et al. RNA imaging. Spatially resolved, highly multiplexed RNA profiling in single cells. Science 2015;348:aaa6090.
[40] Browaeys R, Saelens W, Saeys Y. NicheNet: modeling intercellular communication by linking ligands to target genes. Nat Methods 2020;17:159–162.
[41] Wang MJ, Chen F, Liu QG, et al. Insulin-like growth factor 2 is a key mitogen driving liver repopulation in mice. Cell Death Dis 2018;9:26.
[42] **Luo X**, **Jiang X**, Li J, et al. Insulin-like growth factor-1 attenuates oxidative stress-induced hepatocyte premature senescence in liver fibrogenesis via regulating nuclear p53-progerin interaction. Cell Death Dis 2019;10:451.
[43] Seitz T, Hellerbrand C. Role of fibroblast growth factor signalling in hepatic fibrosis. Liver Int 2021;41:1201–1215.
[44] **Chung WS**, **Shin CH**, Stainier DY. Bmp2 signaling regulates the hepatic versus pancreatic fate decision. Dev Cell 2008;15:738–748.
[45] **Koch PS**, **Olsavszky V**, Ulbrich F, et al. Angiocrine Bmp2 signaling in murine liver controls normal iron homeostasis. Blood 2017;129:415–419.
[46] **Ma M**, **Hua S**, Min X, et al. p53 positively regulates the proliferation of hepatic progenitor cells promoted by laminin-521. Signal Transduct Target Ther 2022;7:290.
[47] Suzuki A, McCall S, Choi SS, et al. Interleukin-15 increases hepatic regenerative activity. J Hepatol 2006;45:410–418.
[48] Russell JO, Monga SP. Wnt/beta-Catenin signaling in liver development, homeostasis, and pathobiology. Annu Rev Pathol 2018;13:351–378.

[49] Santoni de Sio FR, Gritti A, Cascio P, et al. Lentiviral vector gene transfer is limited by the proteasome at postentry steps in various types of stem cells. Stem Cells 2008;26:2142–2152.
[50] Park F, Ohashi K, Kay MA. The effect of age on hepatic gene transfer with self-inactivating lentiviral vectors in vivo. Mol Ther 2003;8:314–323.
[51] Braet F, Wisse E. Structural and functional aspects of liver sinusoidal endothelial cell fenestrae: a review. Comp Hepatol 2002;1:1.
[52] Kumar S, Bandyopadhyay U. Free heme toxicity and its detoxification systems in human. Toxicol Lett 2005;157:175–188.
[53] Yuan X, Fleming MD, Hamza I. Heme transport and erythropoiesis. Curr Opin Chem Biol 2013;17:204–211.
[54] **Guo XL**, **Wang YD**, **Liu YJ**, et al. Author Correction: fetal hepatocytes protect the HSPC genome via fetuin-A. Nature 2025;639:E3.
[55] Hustedt N, Durocher D. The control of DNA repair by the cell cycle. Nat Cell Biol 2016;19:1–9.
[56] Pichard V, Boni S, Baron W, et al. Priming of hepatocytes enhances in vivo liver transduction with lentiviral vectors in adult mice. Hum Gene Ther Methods 2012;23:8–17.

Keywords: liver growth; hepatocyte proliferation; hepatocyte maturation; liver gene therapy; lentiviral vectors; targeted gene editing; single-cell analysis; spatial transcriptomics; tissue niche.
Received 23 August 2024; received in revised form 21 May 2025; accepted 18 June 2025; available online 3 July 2025